An Active Flow Circulation Controlled Flap Concept for General Aviation Aircraft Applications

G. S. Jones, S. A. Viken*, A.E. Washburn*, L. N. Jenkins*, C.M. Cagle***

Flow Physics & Control Branch
NASA Langley Research Center

Abstract

A recent focus on revolutionary aerodynamic concepts has highlighted the technology needs of general aviation and personal aircraft. New and stringent restrictions on these types of aircraft have placed high demands on aerodynamic performance, noise, and environmental issues. Improved high lift performance of these aircraft can lead to slower takeoff and landing speeds that can be related to reduced noise and crash survivability issues. Circulation Control technologies have been around for 65 years, yet have been avoided due to trade offs of mass flow, pitching moment, perceived noise etc. The need to improve the circulation control technology for general aviation and personal air-vehicle applications is the focus of this paper. This report will describe the development of a 2-D General Aviation Circulation Control (GACC) wing concept that utilizes a pulsed pneumatic flap.

Symbols

A	Area (ft^2)
b	Span (inches)
C_L	Lift Coefficient
C_D	Drag Coefficient
C_M	Moment Coefficient
C_μ	Momentum Coefficient
C	Chord (inches)
CCW	Circulation Controlled Wing
D	Drag (lbs)
DC	Duty Cycle (Time On/ Time Off)
E	Mean Voltage
e'	Fluctuating Voltage
h	Slot height (inches)
LE	Leading Edge
L	Lift (lbs)
M	Pitching Moment (in-lbs)
$\dot{m}$	mass flow (lb/sec)
P	Pressure (lb/in^2 or lb/ft^2)
p'	Fluctuating Pressure (lb/in^2 or lb/ft^2)
r	Trailing edge radius (inches)
U	Velocity (ft/sec)
u'	Fluctuating Velocity (ft/sec)
q	Dynamic Pressure (lb/ft^2)
S	Wing plan form area (ft^2)
SCFM	Standard Mass Flow (ft^3/min) (Expanded to 14.7 psia & 72°F)
SPL	Sound Pressure Level (dB)
TE	Trailing Edge
T	Static Temperature (°R)
w	Slot Width (inches)
α	Angle of attack (degrees)
ρ	density (Lbm/ft^3)
Γ	Circulation

Subscripts:

∞	Free stream Conditions
J	Jet at slot exit
o	Stagnation Condition
BAL	Measurements w/ strain gage balance
EQUIV	Equivalent (referenced to drag)

Introduction

In recent years, there has been an increasing interest in revolutionary concepts applied to general aviation and personal aircraft[1] shown in figure 1. New and stringent requirements on these types of aircraft include aerodynamic performance, noise, and environmental issues. The use of Pulsed Pneumatic High Lift Technology has the potential to revolutionize aircraft systems by reducing wing area, reducing part count, lowering weight, and reducing potential runway take off and landing requirements. This paper will give a brief background and review of circulation control physics then describe the development of a 2-D General Aviation Circulation Control (GACC) pulsed wing concept that utilized CFD and wind tunnel experiments.

Figure 1. Artist concept of a personal air vehicle

* RESEARCH ENGINEER
** DESIGN ENGINEER

Background

The definition of "Circulation Control" is strictly related to the circulation characteristics around any aerodynamic body and can be controlled or managed with many different control schemes including airfoil shape and shape change, flaps, ailerons, blowing, suction, etc. Traditionally Circulation Control Wings (CCW) are restricted to a pneumatic modification of the flow field through a Coanda effect.[2] This well known effect was named after Henri Coanda who accidentally discovered it in Paris in 1935. Coanda was trying to deflect the exhaust for an engine only to entrain the hot gas that resulted in destroying the aircraft. This Coanda effect shown in figure 2 can be described by a 2-D wall bounded jet that exits from a slot tangential to a convex curved surface. The wall bounded jet flows along the surface and has the nature of a boundary layer near the wall but becomes that of a free jet at a larger distance from the wall.[3] The degree of jet turning can be related to the slot height, surface radius, jet velocity, and the Coanda surface geometry. The jet turning angle can approach

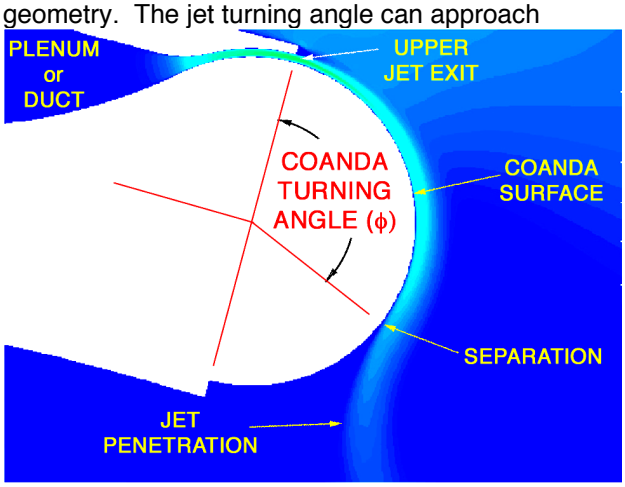

Figure 2 Trailing edge example of Coanda effect

and in some cases exceed 180°. The jet will remain attached to the curved surface because of a balance between the sub-ambient pressure in the jet sheet and the centrifugal force around the curvature of the surface. Although the Coanda effect is very effective for boundary layer control (BLC), the interest in this technology comes from its ability to further augment the circulation and lift with flow turning and control of leading edge streamlines, and thus the name Circulation Control (CC). Lanchester, Kutta, and Joukowski laid the foundation for a quantitative theory relating the lift to an infinite wing through the integration of the velocity field along a streamline.[4]

$$\Gamma = \oint V \cdot dL$$

Where lift is

$$\text{Lift} = \rho \cdot U \cdot \Gamma$$

Once the jet separates from the Coanda surface it penetrates the flow field resulting in a large deflection of the streamlines producing a pneumatic camber similar to a mechanical high lift system, figure 3. The combination of the Coanda separation and the jet penetration will move the rear stagnation point forward on the lower surface and move the leading edge stagnation point aft on the lower surface. As the jet velocity is increased, these stagnation points move toward each other resulting in more circulation. Under ideal circumstances (e.g. circular cylinder) the leading edge stagnation point and trailing edge stagnation point will form a singularity. If the thrust effects from the jet were ignored, this would correspond to a lift coefficient limit of 4π.

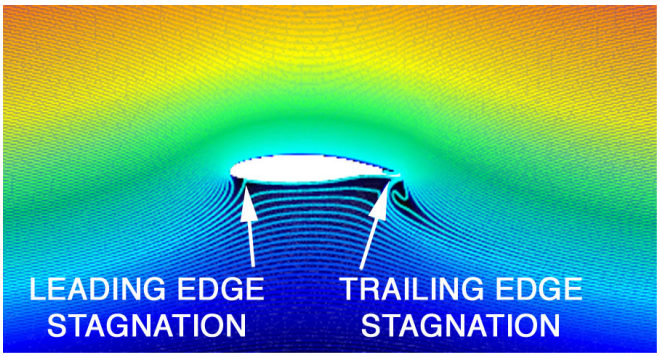

Figure 3 Coanda influence on streamlines

The aerodynamic characteristics of Circulation Control Wings (CCW) have been experimentally and numerically studied for more than 65 years.[5,6,7] Many of these studies have concentrated on trailing edge shape, slot height, and blowing rates. It is obvious that the airfoil shape plays a major role in performance. Various studies utilized airfoil geometries for specific applications such as helicopter rotors, wings, sails, and airfoils with and without camber, etc. Results of these studies highlighted geometric features that affect airfoil performance such as the ratio of the trailing edge radius to chord (r/C), slot height to chord ratio (h/C), slot height to radius ratio (h/r), and Coanda surface shape. In general, the larger the trailing edge radius, the more effective the Coanda effect has on lift due to increased surface area. This is good for the high lift configuration but once the airfoil has reached cruise conditions, there is large drag penalty due to the blunt trailing edge.

It has been found that the use of steady jets, even at very small mass flow rates, yielded lift coefficients that are comparable or superior to conventional high-lift systems. Several CCW high lift studies[8] have shown lift results that approach sectional lift coefficients of 9. This can be compared to traditional mechanical high lift systems that approach maximum lift coefficients of 6 and require complex mechanical systems shown in figure 4. These mechanical systems go beyond the scope of most general aviation aircraft. A more reasonable general aviation high lift system would

be either a simple hinged flap or a single slotted Fowler flap. The lift performance of a typical high lift system is shown in figure 5.[9] Since CCW systems offer such a large potential gain in lift performance, the application to STOL aircraft seems appropriate.

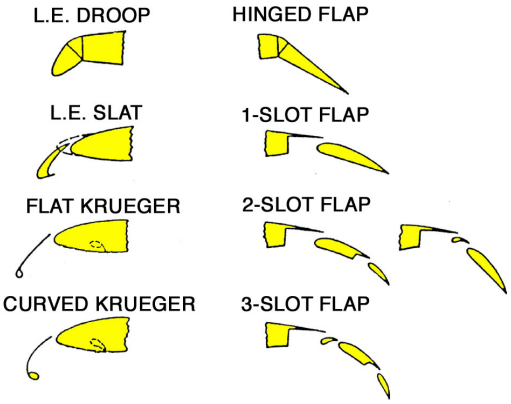

Figure 4. Conventional High Lift Components that a CCW high lift system could potentially replace

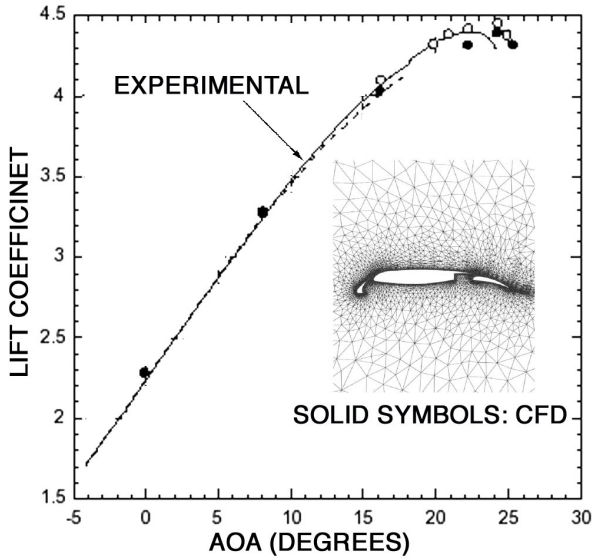

Figure 5. Comparison of computed (FUN2D) and experimental results for three-element airfoil at Mach of 0.20 and Re of 9.x 10^6 (Ref 9)

Through the 1960's and 1980's the U.S. Navy evaluated numerous CCW concepts.[10] To summarize many of these studies and demonstrate the bleed affects associated with CCW, a Circulation Control wing was flight-tested on an A-6 aircraft. This demonstrator showed significant improvements in takeoff and landing characteristics. The maximum lift coefficient went from an un-blown to blown case of 2.1 to 3.9 respectively. The approach speeds decreased from 118 to 76 knots[11].

During the mid-1970's two efforts were completed that focused on pulsed blowing associated with circulation control.[12, 13] Results from these experiments indicated that pulsed blowing reduced the mass requirements for CCW. However both experiments were limited in scope and little was revealed about the physics of the phenomena.

General Aviation Circulation Control

The GACC test program is intended to address technology issues, such as scaling, mass flow, and noise requirements. A 2-D flow physics supercritical airfoil model[14] (figure 6) with dual slotted circulation control capability has been designed and built for low speed testing in the LaRC Basic Aerodynamic Research Tunnel (BART). The primary objective of the program is to evaluate the benefits of pulsed circulation control and to reduce the mass flow requirements for a given lift performance as well as reduce the cruise drag penalty associated with a large circulation control trailing edge.

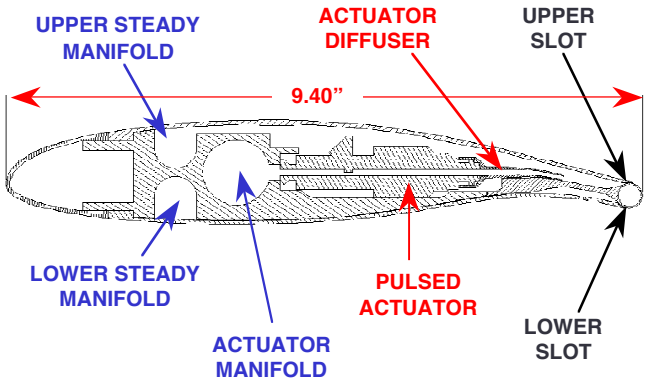

Figure 6. 2-Dimensional 17% Supercritical General Aviation Circulation Controlled Airfoil with a circular trailing edge r/C: 2%

The optimization of high lift and cruise performance with one airfoil shape gives rise to the pneumatic flap concept[15,16] This concept is based on the ability to switch from a high lift configuration to a cruise configuration without utilizing any mechanical systems. Having two independent blowing systems allows one to have such a multi-function system that can be used for high lift systems and flight control systems such as ailerons and air brakes. Moving from a high lift to a cruise configuration is dependent on the upper and lower blowing ratios and the free stream velocity.

As the Coanda effects are modifying the flow-field at the trailing edge, the leading edge stagnation simultaneously moves downstream. This imposes a large pressure gradient at the leading edge that can lead to premature boundary layer separation and airfoil stall. To avoid conventional leading edge slats or other flow control techniques a blunt leading edge is desired. A 17% supercritical airfoil shape based on the GAW(1) was modified at the trailing edge to create the GACC profile. In addition to providing a blunt leading edge this airfoil also provides a sufficient internal volume to house the three pressure manifolds and pulsed actuator.

The GACC model was tested for high lift and cruise configurations by modifying the mass flow through the upper and/or lower slots. Each slot flow was independently controlled and will be discussed later in the text.

Initial testing focused on lift characteristics consistent with general aviation aircraft. A target lift coefficient of 3 was determined to be adequate or exceed most general aviation and personal air vehicle requirements. To determine the experimental test matrix and instrumentation requirements, a 2-D CFD effort was used to quantify flow parameters such as boundary layer separation, slot velocity profiles, mass flow, model surface pressure profiles, internal plenum pressures, lift, drag, and pitching moment.

The two most popular Coanda shapes typically used for CCW applications are based on circular and elliptic profiles. For low speed applications such as high lift, the circular profile is more effective than the elliptic shape. However the elliptic shape is more effective at high-speed cruise conditions than the circular shape.

A 2% r/C circular trailing edge shape was chosen as a baseline for the GACC model. The trade off of high lift performance and cruise drag is based on optimizing the high lift system first then utilizing the dual blowing to optimize the cruise drag.

Theoretical Considerations

The momentum coefficient Cμ is a critical parameter in understanding the efficiencies of blown systems such as the GACC and is defined as

$$C\mu = \frac{Thrust}{qS} = \frac{\dot{m}(U_J)}{q(C)(b)} \quad \text{(Eq.1)}$$

where

$$\dot{m} = \rho_J U_J A_J \quad \text{(Eq.2)}$$

and

$$U_J = \sqrt{\frac{2\gamma R(T_{DUCT})}{\gamma - 1}\left(1 - \left(\frac{P_\infty}{P_{DUCT}}\right)^{\frac{\gamma-1}{\gamma}}\right)} \quad \text{(Eq.3)}$$

It should be noted that the jet velocity has been expanded isentropiclly to free stream conditions and is in general less than the centerline jet velocity at the exit of the nozzle as will be shown later in the text. The momentum coefficient can be expanded to become:

$$C\mu = 2\left[\frac{(h)(w)}{(C)(b)}\right]\left(\frac{\rho_J}{\rho_\infty}\right)\left(\frac{U_J}{U_\infty}\right)^2 \quad \text{(Eq.4)}$$

Since the jet velocities are expected to be compressible, the density ratio will be based on the Mach number related to equation 3. Figure 7 highlights the non-linearity of the momentum coefficient due to the density ratio.

Using the momentum formulation described above does not accurately characterize the physics related to airfoil performance for different slot heights. Nominally smaller slot heights yield a larger return in lift coefficient at constant Cμ than do larger slot heights. An empirical technique[6] described by equation 5 is often used to collapse the performance data.

$$C\mu_{BLC} = C\mu\left[1 - \sqrt{1 - Cp_J}\left(\frac{U_\infty}{U_J}\right)\right] \quad \text{(Eq.5)}$$

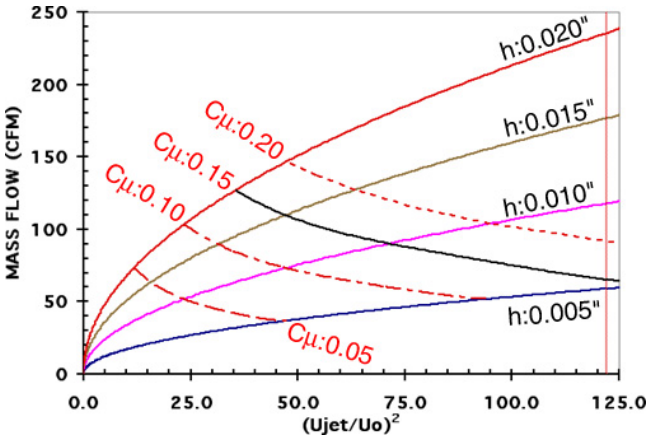

Figure 7. Mass flow requirements for a circulation control wing at a q: 10 psf and To: 75°F.

Pulsed theoretical considerations

For the time dependent pulsed flows the jet velocity will be divided into a mean and fluctuating component.

$$U_J = \overline{U_J} + u_J' \quad \text{(Eq.6)}$$

Substituting into equation 4 the total momentum coefficient becomes:

$$C\mu = \overline{C\mu} + C\mu' \quad \text{(Eq.7)}$$

where

$$C\mu' = 2\left[\frac{(h)(w)}{(C)(b)}\right]\left(\frac{u_J'}{U_\infty}\right)^2 \quad \text{(Eq.8)}$$

and

$$\overline{C\mu} = 2\left[\frac{(h)(w)}{(C)(b)}\right]\left(\frac{\overline{\rho_J}}{\rho_\infty}\right)\left(\frac{\overline{U_J}}{U_\infty}\right)^2 \quad \text{(Eq.9)}$$

Equation 8 assumes that the 2nd order influence of the unsteady density ratio can be neglected (i.e. ignoring compressibility effects and cross correlation terms). Figure 8 illustrates a pulsed jet having a 20% duty cycle and the potential demand for actuator authority, (the magnitude required to influence for flow field). Even if an ideal pulsed jet can be created, it will become distorted at the exit plane due to the compressible effects that are related to the volume of the plenum. As this distortion occurs the demand on time accurate measurements at the slot exit become more important in understanding the physics of the pulsed circulation system.

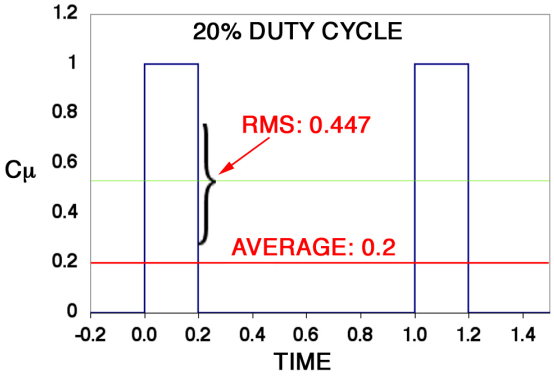

Figure 8. Example of a theoretical pulsed jet

Experimentally many researchers are not always able to make detailed and accurate measurements at the jet exit due to large velocity perturbations and/or small scales. Measurements in the plenum or upstream of the model are often used to quantify mass flow and jet velocity to "standard" or free stream conditions. This also enables the researcher to manage the density ratio more effectively. If the mass flow measurements are made far enough upstream, the perturbations are damped and the total mass flow conditions are captured. Equation 1 then becomes:

$$C\mu = \frac{\dot{m}\left(\overline{U_J} + u'_J\right)}{q(b)(C)} \quad \text{(Eq.10)}$$

where the mean and fluctuating velocities can be obtained from equation 11 and 12.

$$\overline{U_J} = \sqrt{\frac{2\gamma R(T_{DUCT})}{\gamma - 1}\left(1 - \left(\frac{P_\infty}{P_{DUCT}}\right)^{\frac{\gamma-1}{\gamma}}\right)} \quad \text{(Eq.11)}$$

$$u'_J = \sqrt{\frac{2\gamma R(T_{DUCT})}{\gamma - 1}\left(1 - \left(\frac{P_o}{p'_{LOCAL}}\right)^{\frac{\gamma-1}{\gamma}}\right)} \quad \text{(Eq.12)}$$

In addition to eliminating the issues associated with density ratios, this approach also eliminates the errors associated with the measurement of the slot height.

The influence of the Coanda jet on the non-dimensional lift, drag and pitching moment are realized in the forces created on the airfoil. It is necessary to define an equivalent drag for an airfoil that has a potential for creating thrust. This enables blown sections to be comparable to conventional airfoils and avoids lift to drag ratio (airfoil efficiency) from going to infinity as the measured drag approaches zero due to blowing.[17] A single force-based coefficient simply includes the momentum coefficient to the measured drag coefficient.

$$C_{D(EQUIV)} = C_{D(BAL)} + C\mu \quad \text{(Eq13)}$$

Perhaps a more appropriate parameter is a kinetic energy based correction that is expressed as:

$$C_{D(EQUIV)} = C_{D(BAL)} + C\mu\left(\frac{U_J}{2U_\infty}\right) \quad \text{(Eq.14)}$$

To include an additional penalty for mass intake (ram effect) results in:

$$C_{D(EQUIV)} = C_{D(BAL)} + C\mu\left(\frac{U_J}{2U_\infty}\right) + C\mu\left(\frac{U_\infty}{U_J}\right) \quad \text{(Eq.15)}$$

Comparisons of these correction techniques are shown in figure 9 by highlighting the components being added to the measured drag. Nominally the momentum coefficient is small for cruise conditions resulting in a minimal impact of the correction technique. As the momentum coefficient increases for high lift conditions at low speed, the selection of the correction technique becomes more critical. Of the three equivalent drag techniques, the kinetic-energy based term coupled with the mass intake penalty is the most conservative and best represents the physics related to the drag and will be used throughout remainder of this text unless otherwise noted.

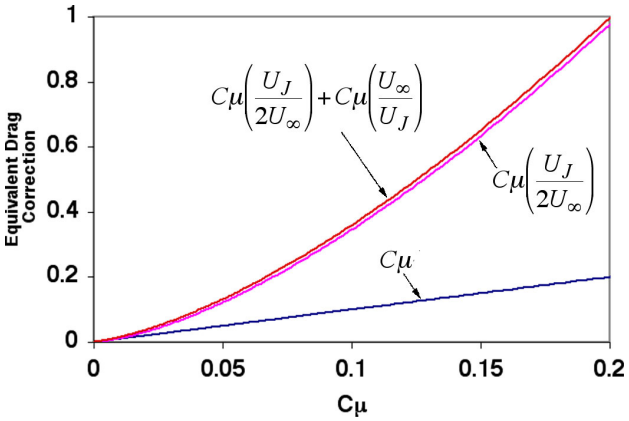

Figure 9 Comparison of equivalent drag correction techniques

CFD Analysis

The NASA LaRC **F**ull **U**nstructured **N**avier-Stokes 2D code (FUN2D) was used for the CFD computations. The flow solver is a node based, implicit, upwind flow solver used for computing flows around single or multi-element airfoil configurations with unstructured grid.[18] The governing equations are the time-dependent Reynolds-Averaged Navier-Stokes (RANS) equations in conservation-law form, which are integrated in time to obtain a steady state solution. The Spalart-Allmaras turbulence model[19] was used in this investigation and all computations assume fully turbulent flow. Boundary conditions that enable blowing capability were integrated into the code. Steady jet calculations were performed over a range of slot heights, blowing rates, and angles of attack.

The grids were generated with advancing front type point placement with iterative local re-meshing for grid quality improvement.[20] [21] The outer boundaries

were treated as characteristic inflow and outflow surfaces and extended 20 chord lengths in all directions from the leading edge of the model. No-slip viscous boundary conditions were prescribed on the airfoil surface and the blowing boundary conditions were applied to a vertical plane internal to the model.

For a chord Reynolds number of 533000, the turbulent minimum normal wall spacing on the airfoil was set to 2.0 x 10^{-6} based on a chord of 1.0. The grid generated for the GACC airfoil consisted of 90,582 nodes with 1540 nodes on the airfoil surface and the duct walls. Figure 10a shows the unstructured grid generated around the GACC model. Figure 10b shows an enlarged view of the grid in the duct region, highlighting the blowing boundary condition that coincides with the exit plane of the actuator rapid diffuser.

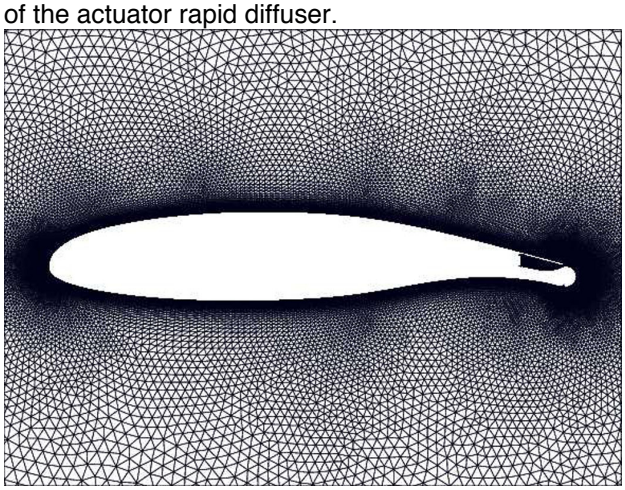

a) Unstructured grid for GACC airfoil

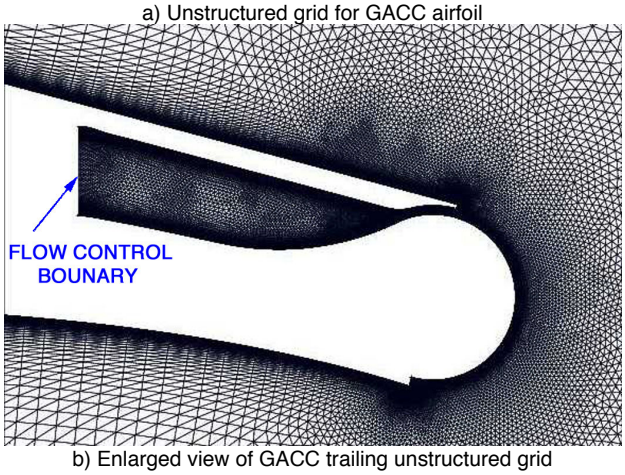

b) Enlarged view of GACC trailing unstructured grid

Figure 10 FUN(2D) grid for GACC airfoil high lift configuration with a slot height of 0.020"

The initial expectations of the CFD effort were built around using the code as a tool for designing the experiment. To gain confidence in the application and use of the code in the GACC research program, a test case was run for a GAW(1) airfoil. A comparison of GAW(1) lift coefficient data with two independent experimental studies[22, 23] showed favorable results, (figure 11).

The GACC airfoil used throughout this study was a modified GAW(1) airfoil. This modification occurs only on the under surface near the trailing edge to accommodate the 2% r/C Coanda surface. The chord reference line used for angle of attack extends along the original GAW(1) leading and trailing edge references. For the GACC airfoil this

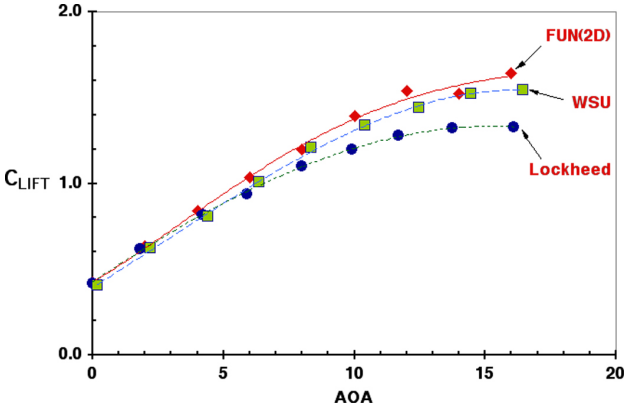

Figure 11.FUN(2D) validation using GAW(1) experiments

corresponds to the same leading reference and a trailing edge reference that is tangent to the upper Coanda surface coinciding with the upper surface jet exit plane.

Initial studies of the Coanda turning revealed the need to model the internal plenum due to discontinuities at the slot exit and difficulties with convergence. The internal GACC plenum to jet exit contraction ratio varied from 10:1 to 20:1 depending on the slot height. The magnitude of the jet velocity was controlled at the internal boundary corresponding to the exit of the actuator.

The predicted lift performance of the GACC airfoil shown in figure 12 is consistent with similar supercritical airfoils.[24] Sequences of flow fields with varying blowing rates are shown in the appendix. The visible boundary shown in this sequence is

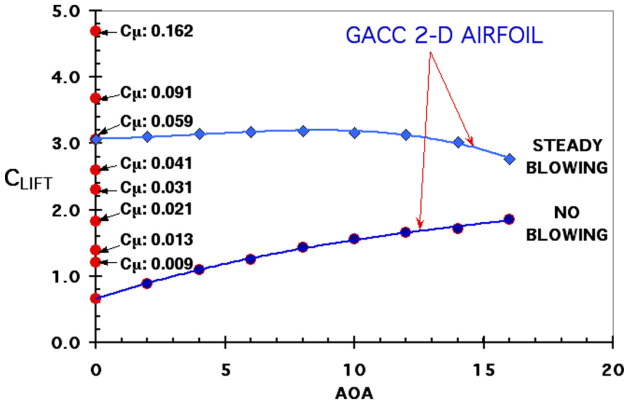

Figure 12 GACC predicted performance using FUN(2D)

representative of the wind tunnel walls and shows the potential wall interference effects. As the jet velocity increases, the Coanda turning angle also increases until

it reaches a limit imposed by the GACC's lower slot exit. The Coanda jet penetrates the low momentum wake and deflects the streamlines near the trailing edge. As the jet velocity continues to increase, the Coanda jet penetrates the flow at a fixed angle. The vectored jet departs the Coanda surface into the oncoming flow field, creating a negative thrust (e.g. similar to a thrust reverser). The degree of penetration is dependent on the magnitude of the jet exit velocity and free stream velocity. As the jet penetrates the flow field and turns the streamlines the effective pneumatic flap is created.

The corresponding pressure profiles shown in figure 13 highlights the pitching moment created

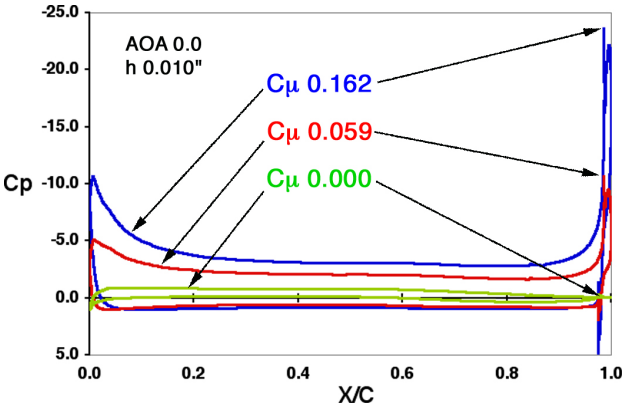

Figure 13 GACC pressure profile for varying momentum coefficients (0<Cμ<0.2), Mach 0.1

by the large velocity at the jet exit. Looking closer at the trailing edge reveals a large pressure difference across the jet exit shown in figure 13. This is characteristic of a wall-bounded jet. Caution must be given in using the pressure data from the Coanda surface to estimate the jet velocity at the exit as will be discussed.

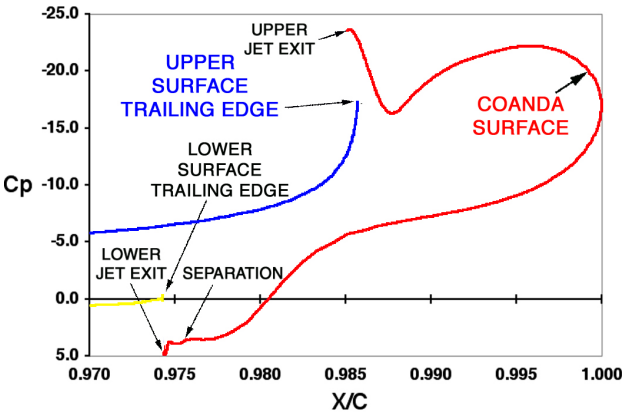

Figure 13. Trailing edge pressure distribution along the Coanda surface for Cμ 0.162, Mach 0.1, AOA 0.0, and h/C 0.001.

Examining the same profile relative to the Coanda surface shown in figure 14, reveals the wall-bounded jet decelerating as the low momentum outer flow is entrained near the jet exit. It then briefly accelerates and remains attached to the Coanda surface until confronted with the forward facing step of the lower jet exit plane. The large suction peak at the trailing edge significantly

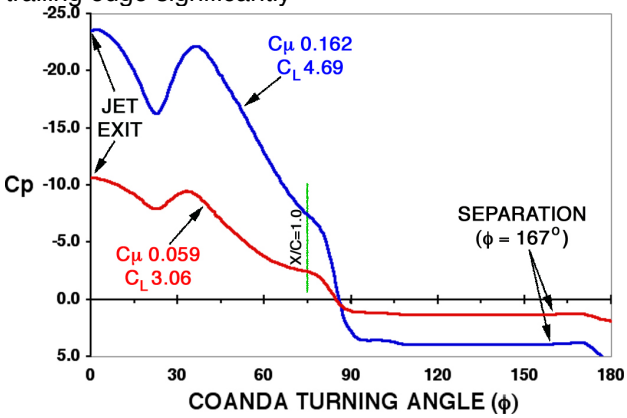

Figure 14 Comparison of two pressure profiles along the Coanda surface

contributes to increasing the lift, drag, and pitching moment.

The Mach number profiles at the jet exit are consistent with a developing internal nozzle flow field as shown in figure 15. If one uses the static pressure at the exit plane on Coanda surface (peak pressure shown in figure 13) the resulting Mach number will be inconsistent with the centerline Mach number of the Coanda jet. The use of the jet velocity based on the

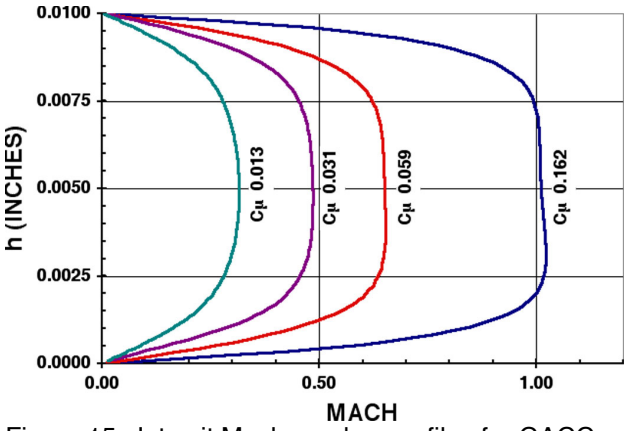

Figure 15. Jet exit Mach number profiles for GACC h:0.010", free stream Mach:010.

centerline Mach number to calculate the momentum coefficient will result in an over-prediction of the momentum due to losses associated with the growing internal boundary layers. This is particularly true for smaller slots where the nozzle boundary layers are a significant portion of the jet flow field. Therefore, integration of the jet profile is necessary. Nominally this will result in a lower jet velocity magnitude. This may explain why using free stream static pressure (isentropic

expansion of jet) to calculate the Coanda jet velocity has been historically successful in momentum calculations.

Experimental Setup

The development of the GACC test program is based on a pulsed circulation control concept. Actuator authority and frequency response are characterized by state of the art high-speed valves and are the cornerstone to the model development. The model requirements were established to provide baseline and unsteady circulation control data for proof of concept and code validation of pneumatic flap and control surface concepts.

Actuator Description

Studies that have attempted pulsed circulation control have historically been limited to rotary or shuttle valves and have had limited authority and frequency response. Requirements for the current study were to extend the frequency survey to 200 Hz with peak velocities that approach sonic conditions. Pulsed actuation can be generated through valving the flow path to the trailing edge. While it is convenient to place the valve system outside the model, the frequency response will decay as a result of the volume and flow path leading to the jet exit at the trailing edge. To minimize this decay and avoid unwanted 3-D effects, it is important to locate the valve system as close to the jet exit as possible. This requirement lead to the development of a high-speed solenoid operated valve system that would be distributed along the span of the GACC model.

Figure 16 shows an example of a high-speed solenoid operated valve. This valve utilizes a piston that seats into an 0.010-inch orifice, and is cycled from a full open to a full closed condition. This enables the valve to generate a pulsed flow with variable frequency, duty cycle, and velocity magnitude.

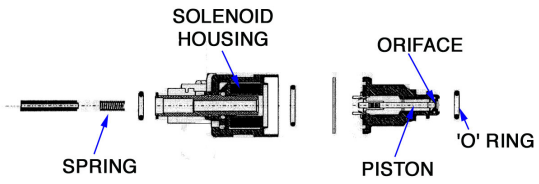

Figure 16 Breakdown of a high-speed solenoid valve.

The calibration of a single actuator provided information that was used to size the high pressure air delivery system and quantified the number of actuators required to meet the mass flow requirements necessary to achieve the target lift coefficient. The mechanics of the piston-spring system that is internal to the actuator showed a 15% reduction as the frequency increased from 25Hz to 100Hz, figure 17.

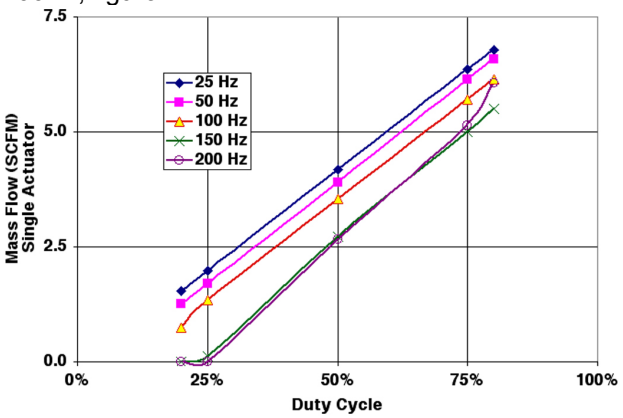

Figure 17 Actuator mass flow authority of a high-speed solenoid valve operated at different duty cycles and frequencies. Inlet pressure 200 psig.

Assuming that a $C\mu$ of 0.1 is required to achieve the desired lift, 100 SCFM will be required of the actuator system, see figure 7. Figure 18 shows the electronic timing associated with a typical injector. The hot wire location had to be moved one inch downstream as the high velocity pulsed stream kept breaking wires.

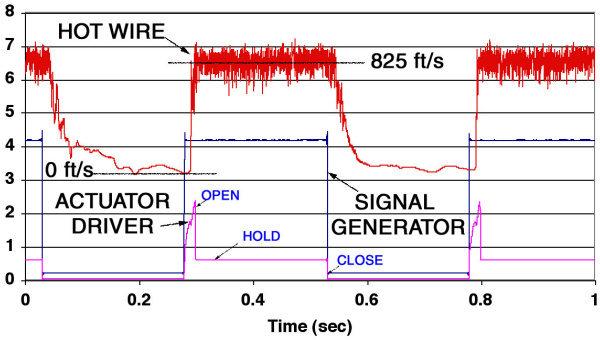

Figure 18 Comparison of the timing of the pulsed actuator system, frequency: 20 Hz, DC 0.50, Inlet pressure 200 psia.

Evaluating the general performance of a single actuator (tables 1 through 3) one can see that 20 actuators will be required to operate simultaneously at 5 SCFM to meet the 100 SCFM imposed by the lift requirement. It is clear that not all frequencies and duty cycles meet this requirement.

Actuator Rapid Diffuser Description

The flow field out of the actuator is a small diameter circular high-speed jet. To avoid unwanted 3-D span-wise flows it was necessary to design a rapid diffuser that could be integrated into the GACC model. The objective of the diffuser is to transition from a circular, time-dependent, high-speed jet to a low speed 2-D, uniform jet. This was accomplished with a 10:1 area ratio diffuser shown in figure 19.

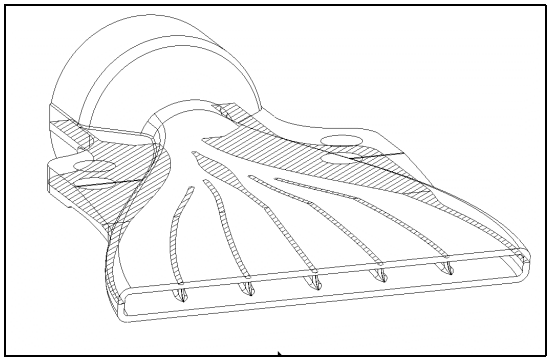

Figure 19. Rapid diffuser with internal guide vanes for GACC Actuator.

Model Description

The GACC model was designed around the pulsed actuation system and sized to fit into the LaRC BART wind tunnel. The model is a 17% thick supercritical airfoil that has a 9.4-inch chord and a 28-inch span (aspect ratio 2.98). There are 20 independently pulsed actuators distributed along the span of the model, figure 20. The model is mounted vertically through the tunnel floor and spans the entire height of the tunnel.

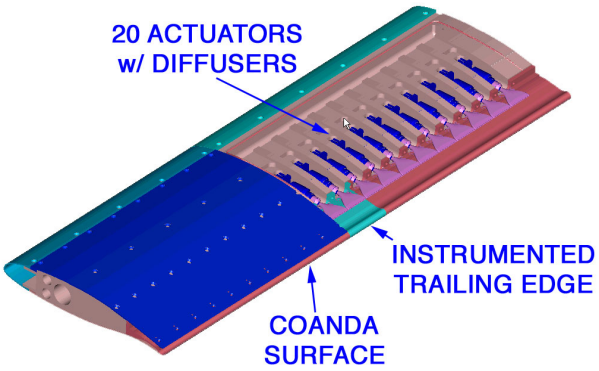

Figure 20. GACC Model w/ upper surface removed to expose internal actuator system

To accommodate the 5 component balance system the model was cantilevered and a 0.125-inch gap was left at the ceiling to avoid fouling. The 5-component GACC strain gage balance was designed around the lift and drag performance predicted by the CFD analysis. Since the model was mounted vertically, the gravity direction was ignored. A description of the balance limits is shown in table 4.

The model design also accommodated one high pressure and two low-pressure air supply lines that were coupled to the air delivery system through a trapeze[14]. The trapeze was fabricated with flexible hoses that minimized the forces transmitted to the model. The tare forces associated with the air supply system were statically calibrated then applied real time to the force data.

The balance had natural frequencies of 12.7 Hz and 78.6 Hz for the axial and normal components respectively. These frequencies were avoided by driving the pulsed actuator system at frequencies above or below the predicted natural frequencies. The axial component was easily excited, even with steady blowing conditions. This limited the test matrix and increased the errors associated with drag measurements for certain conditions. Figure 21 shows the assembled GACC model system.

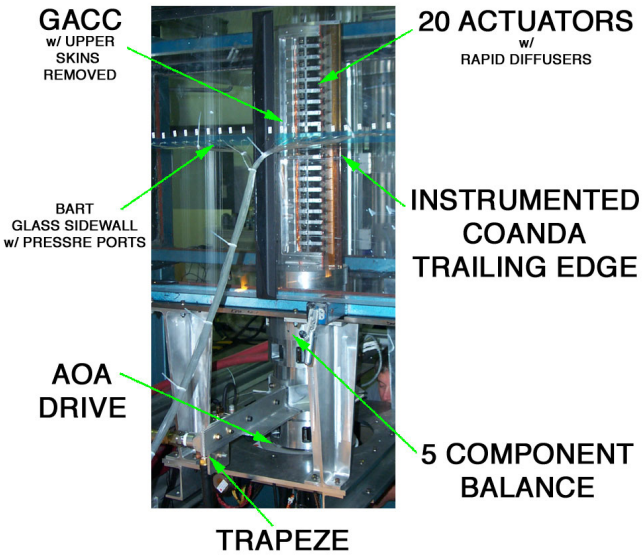

Figure 21. Photograph of GACC model assembly

An electronically scanned pressure system was used to measure 52 steady model pressures and 150 wind tunnel wall pressures. Two 32-port modules were mounted internal to the model to avoid balance interference. The trailing edge Coanda surface was instrumented with 40 thin films and 13 unsteady surface pressure transducers shown in figure 22.

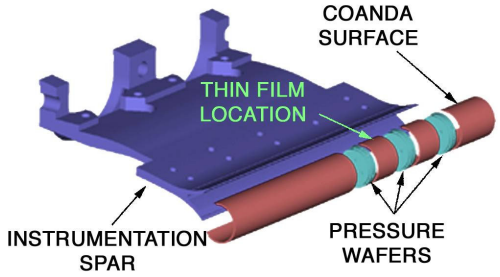

Figure 22. Trailing edge instrumentation package for all test conditions.

Each pressure wafer had multiple independent 0.020” 5-psig pressure sensors bonded to the surface. During the course of testing it was discovered that a small pressure leak developed at the interface of a pressure wafer and the instrumentation spar. This biased the mean pressure measurements but was assumed to have a minimal impact on the fluctuating pressure measurements due to the slow leak rate.

The GACC air supply system design, figure 23, was based on a $C\mu$ that would be limited to 0.2 or less.

This corresponds to a maximum mass flow of 150 SCFM (see figure 7) and enables the researcher to test through predicted lift coefficients of 4.5 for different slot geometries. Two of the air supply systems were designed to provide independent control of both upper and lower steady blowing. Each of these independent systems was limited to 30 psig of controlled steady air to the isolated upper and lower plenums. The third air supply system supplied the actuator manifold with a regulated pressure that ranged from 50 psig to 200 psig. The mass flow for each of the air supply lines was independently measured at the exit of the air supply system with turbine type flow meters. The actuator line was buffered with a surge tank to avoid pressure pulses back to the flow metering system. A detailed description of the GACC model design can be found in Reference 13.

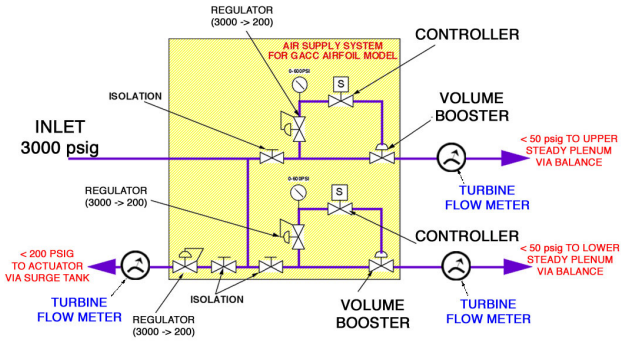

Figure 23. Schematic of GACC air supply system

Facility Description (BART)

The NASA-Langley Basic Aerodynamics Research Tunnel (BART) is a flow-diagnostic facility that specializes in the acquisition of detailed data for the development and validation of CFD models and advanced flow diagnostic techniques. Its flexibility and advanced measurement capabilities are often utilized to investigate the fundamental characteristics of complex flow fields about various vehicle configurations.

BART is a subsonic, open-return wind tunnel with a closed test section 28 inches high, 42 inches wide and 120 inches long. During operation, air is drawn into the tunnel inlet under atmospheric conditions by a 9 blade-11 stator fan. The fan is powered by a 125 horsepower, alternating current motor coupled to a magnetic clutch. Air passes through a honeycomb, four anti-turbulence screens, and an 11:1 contraction before entering the test section. The maximum velocity at the test section entrance is 186 ft/s, which corresponds to a unit Reynolds Number (Re/ft) of 1.13 million and a dynamic pressure of 40 lf/ft^2. The turbulence intensity varies from 0.03% at 50 ft/s to 0.09% at tunnel maximum velocity.

Experimental Analysis

The evaluation of the GACC performance is broken into three separate efforts, 1) baseline high lift performance using steady blowing, 2) cruise performance using simultaneous upper and lower steady blowing, and 3) high lift performance using pulsed blowing. Two GACC slot geometries were tested (h/r: 0.0533 and 0.1067) and selected data will be presented. Wall interference corrections have not been applied to any of the experimental data.

1) Baseline High Lift Performance

To capture the details of the physics associated with circulation controlled concepts it is often beneficial to step back and look at the global picture. A flow visualization experiment was performed to provide real time flow analysis. A separate and smaller GACC model was designed and built for water tunnel applications. Figure 24 is an example of a hydrogen bubble flow visualization technique used to evaluate the flow turning of the GACC model. Movies highlighted both positive and negative high lift characteristics as well as the cruise condition.

(a) No Blowing

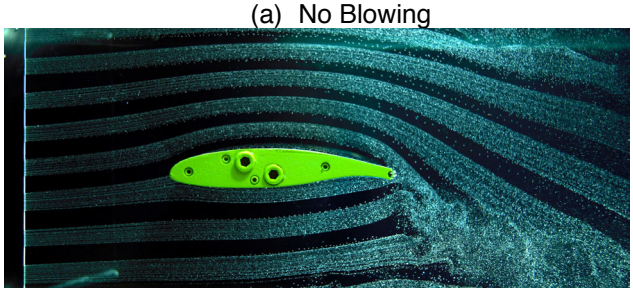

(b) Upper Surface Blowing

Figure 24. Hydrogen bubble flow visualization of the GACC airfoil.

The flow visualization experiment highlighted several important features of the GACC model, such as

- 3-D slot flow can be generated without appropriate internal flow conditioning resulting in inefficient flow turning,
- velocity ratios near 1 are the most efficient for the dual blowing cruise conditions, and
- tunnel walls can become separated with high degrees of flow turning that are characteristic of circulation control wings.

BART High Lift Performance

The high lift performance will be discussed in two separate sections; a) positive high lift (Upper surface blowing) and b) negative high lift (Lower surface blowing)

a) Upper Surface Blowing

The baseline performance of the GACC model is characterized by the lift and lift efficiency (L/D) shown in figures 25. The GACC experimental lift results evaluated at an angle of attack of zero will provide lift augmentation, $\Delta C_L/\Delta C\mu = 50$. This is consistent with other small trailing edge CCW airfoil experiments.

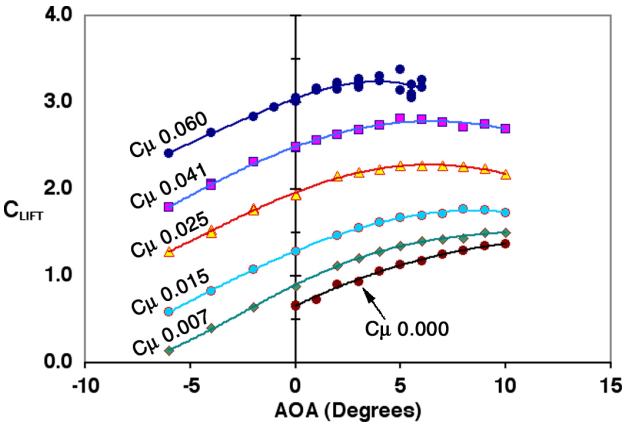

Figure 25 Lift characteristics of the 2-D GACC airfoil

There is a favorable comparison of the CFD and experimental pressure data as shown in an example in figure 26.

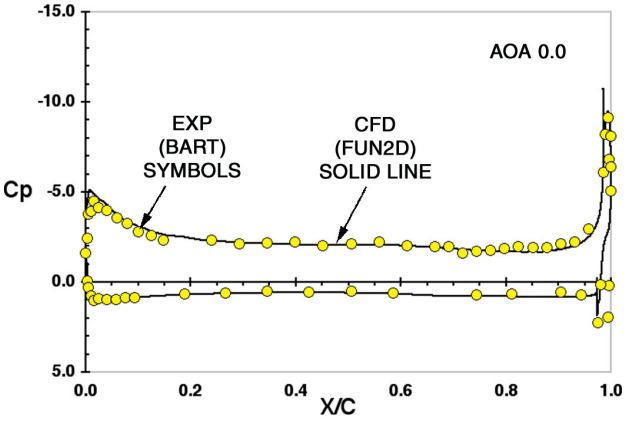

Figure 26 Comparison of CFD and experimental pressure for the GACC airfoil, h 0.010" Cμ 0.06

The differences in the trailing edge pressures are highlighted in figure 27. While the trends are similar, the confidence in the experimental pressures is limited due to a slow pressure leak into the reference plenum that developed during the test.

Due to the lack of confidence in the unknown trailing edge pressure and the associated error magnitudes, pressure data could not be used to obtain force data that would compliment the balance

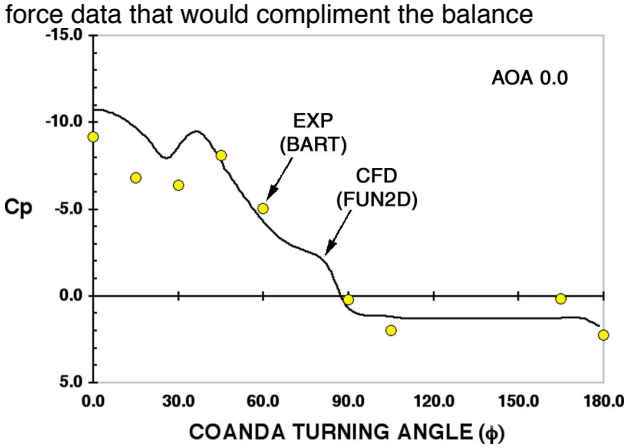

Figure 25 Comparison of CFD and experimental Coanda pressure distribution for the GACC airfoil, h 0.010", nominal Cμ 0.06

data. This also made corrections to the momentum coefficient (equation 5) impractical since the measured pressure at the jet exit was unreliable. Therefore, the momentum data for the CFD and experimental results are both based on equations 1 and 3. This would suggest that there will be a potential difference in the described lift performance for the different slot heights.

CFD predicted the GACC experimental performance trends for the small slot configuration very well, as shown in figure 26. As noted above, the lift performance for the different slot heights should be different as demonstrated with the CFD data shown in figure 26. However, this trend is not realized in the experimental data and is not understood at this time.

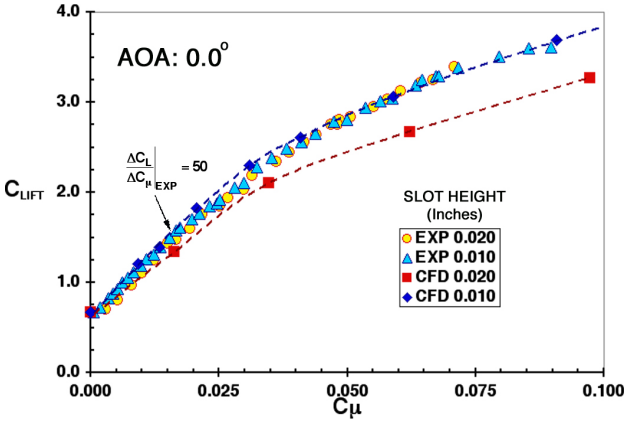

Figure 26 Comparison of CFD and experimental Lift characteristics of the 2-D GACC high lift airfoil configuration.

The drag polar for the GACC high lift configuration at zero degrees angle of attack is shown in figure 27. The general trend is consistent with performance characteristics of traditional high lift systems that vary in angle of attack. However, the CFD results are lower than the experimental data and may be

a result of the experimental wall interference, balance errors, mass flow measurement errors, and/or errors in setting the slot height of GACC model.

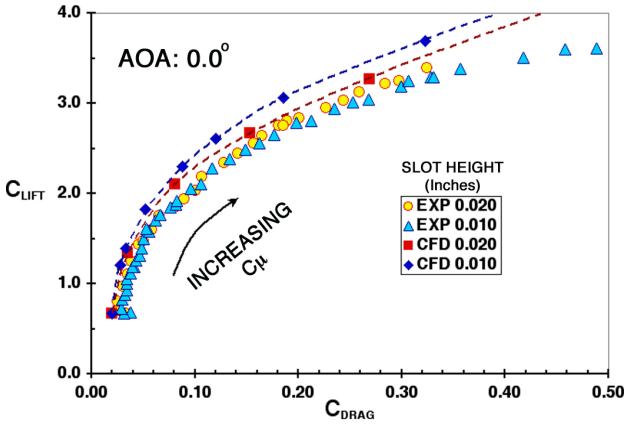

Figure 27. Drag Polar for GACC 2-D high lift airfoil configuration using Equivalent Drag (0<Cμ<0.10)

The airfoil efficiency for the GACC airfoil at zero degrees angle of attack is shown in figure 28. The trends can be compared to conventional high lift systems described by C.P. van Dam.[25] While the overall airfoil efficiency of a conventional airfoil system is higher than the GACC airfoil shown here, there remain questions regarding the uncertainties related to the kinetic energy components added to the balance data.

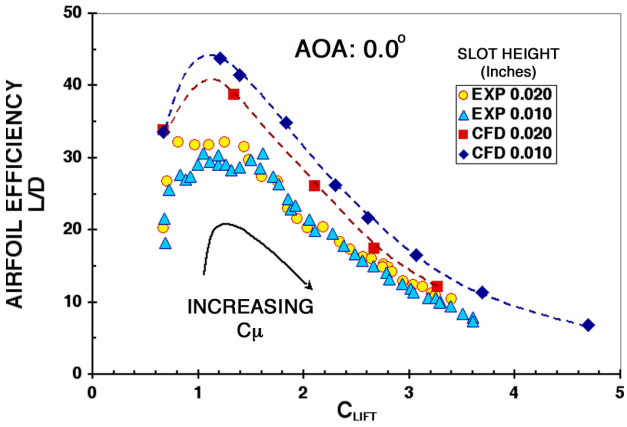

Figure 26 Airfoil efficiency (L/D) of a 2-D GACC high lift airfoil configuration

b) Lower Surface Blowing

A unique feature of the GACC airfoil is its ability to generate negative lift by blowing from the lower slot. While one may question usefulness of this configuration, it has the potential to make rapid flight path corrections depending on the frequency response of the system. The momentum requirements of the negative lift configuration are shown in figure 27. The stall characteristics occur at a momentum coefficient of approximately 0.05 with a maximum negative lift of –1.0.

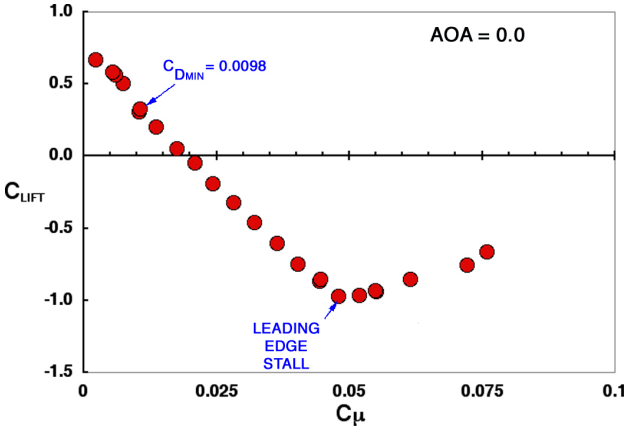

Figure 27 Lift performance of GACC 2-D airfoil negative lift configuration (Lower Surface Blowing) (AOA:0.0)

The drag polar of the negative lift configuration decreases from the un-blown baseline, figure 28. Comparing the minimum drag of the upper blown high lift configuration shows a small improvement in the minimum drag for the negative high lift configuration. Using lower surface blowing one can optimize the cruise drag for a given lift coefficient, (eg. C_L 0.25 and C_{Dmin} 0.0098 are typical for a general aviation aircraft)

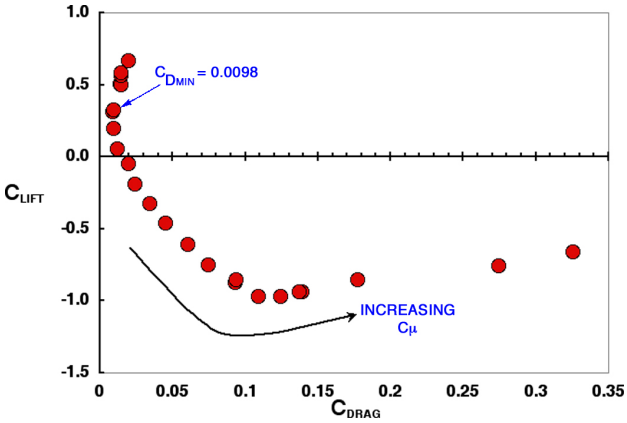

Figure 28 Drag Polar for a GACC 2-D airfoil negative lift configuration (Lower Surface Blowing) (AOA:0.0)

c) Dual Blowing

The combined or dual blowing configuration of the GACC airfoil is targeted at understanding the minimum blowing requirements for cruise conditions of a CCW airfoil. For cruise conditions the ratio of the jet velocity to free stream velocity is a critical parameter. As the free stream velocity increases to high subsonic speeds, the jet velocity required for optimal cruise will also increase. It is important to keep the interactions with any shock formations to a minimum. For this series of experiments the free stream velocity was kept low to avoid compressible conditions. Figure 30 highlights the uncorrected drag and the measured thrust for two slot configurations at zero angle of attack. The larger slot

develops more thrust vectoring as a result of increased mass.

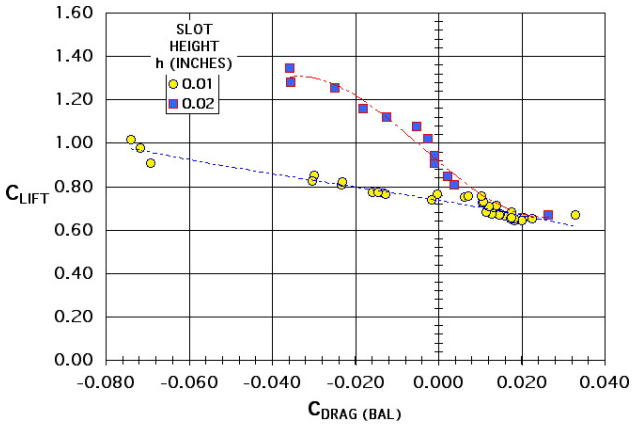

Figure 30 Dual Blowing Influence of two slot heights (Balance data)

The drag polar shown in figure 31 illustrates a significant benefit of the dual blowing configuration. A 38% reduction in drag occurs at a –4° angle of attack and velocity ratio of 1.2 shown in figure 32.

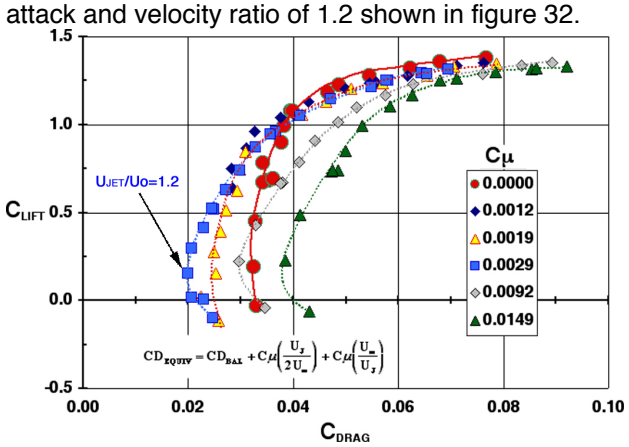

Figure 31. Dual Blowing Drag Polar (h: 0.01)

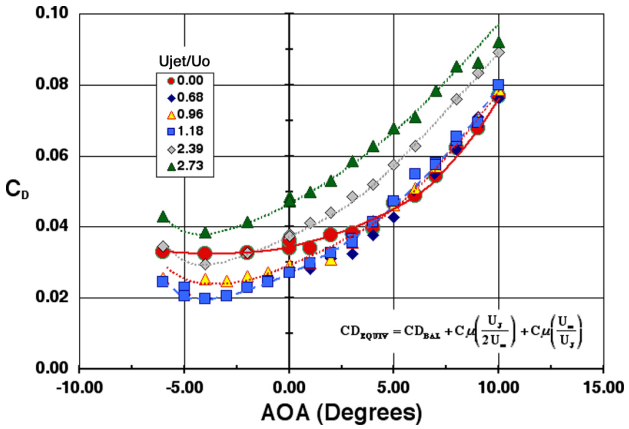

Figure 32. Drag performance of the GACC airfoil for different velocity ratios.

The trends in dual blowing efficiency, shown in figure 33, are low compared with the peak efficiencies of conventional airfoil cruise configurations. This is due to the high drag values being influenced by the kinetic energy and momentum effects.

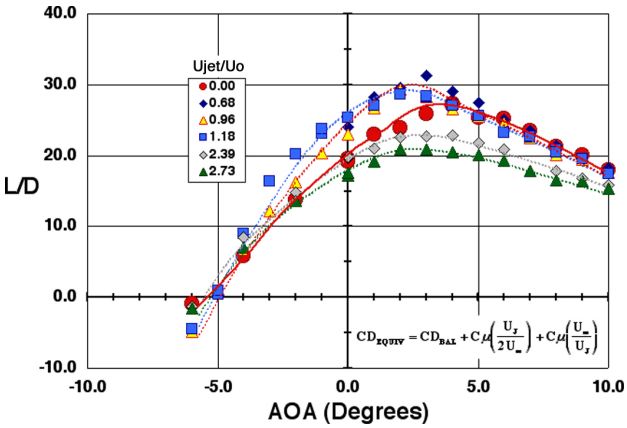

Figure 33. Dual Blowing Lift to Drag ratio (h: 0.01)

d) Pulsed Blowing

The effectiveness of pulsed blowing on the performance of the GACC airfoil is dependent on the efficiency of the actuator system. This system must include the actuator performance, diffuser performance, and the response of the internal volume prior to the jet exit as well as the external time dependent Coanda effectiveness. Ideally the time dependent Coanda response would resemble the steady state blowing series shown in the appendix. This would assume a perfect square wave response at the jet exit. The reality of a perfect square wave diminishes with the complexities of the actuator system.

The response of the state of the art high-speed actuator valves used for this study does not generate a perfect pulsed[26] waveform as typified in figure 16. Transmitting the pulse through the nozzle and into the nozzle exit distorts the waveform further as shown with thin film data located at the nozzle exit. For the low frequency pulsed jet, the effect of duty cycle is shown in 34. The peak amplitude for the low duty cycle conditions (20% and 30%) does not reach the maximum output performance of the actuator system. This result is caused by the actuator valve being closed before the plenum and actuator volumes have had time to be fully pressurized. Once the valve is given a close command the plenum remains pressurized and continues to bleed air through the jet exit until the plenum pressure reaches ambient conditions.

As the drive frequency is increased, figure 35, the rise time or valve opening distortions increase. For the closed portion of the duty cycle, air continues to bleed from the plenum until the open command is given, resulting in the jet velocity not going to zero. This process limits the mass flow to the jet exit as indicated by an overall reduction in the peak velocity. In spite of

the limitations of the actuator system, the peak velocities do approach sonic conditions.

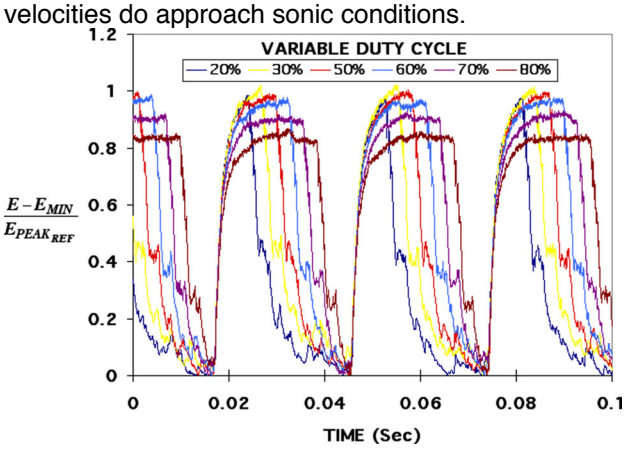

Figure 34 Normalized thin film time history for pulsed CCW at the slot exit. (h: 0.020 and Driver Frequency: 35 Hz)

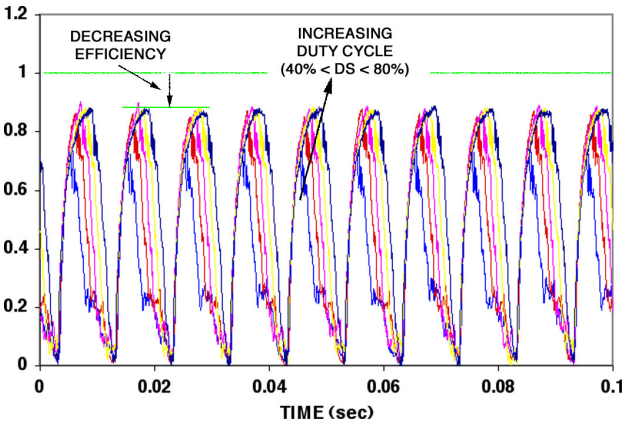

Figure 35 Normalized Thin Film Time histories for pulsed CCW at the slot exit, (h: 0.020 and Driver Frequency: 100 Hz)

Figure 36 illustrates the authority of the pulsed jet on the Coanda surface. The magnitude of the jet decreases as the flow exits the nozzle and moves along the Coanda surface. It is important to recognize the structure of the pulsed waveform is maintained until the flow separates from the Coanda surface.

As the pulsed flow exits the nozzle, a large increase in the turbulence characteristics are observed. The spectra of two surface thin films near the nozzle exit are shown in figure 37. These data are consistent with conditions measured for both slot configurations. For low frequency pulsed jets, the frequency characteristics of the jet can be separated into pulsed and turbulence regimes. The transition from the pulsed to the turbulence regime seemed to be independent on the jet velocity and occurred near 300 hz.

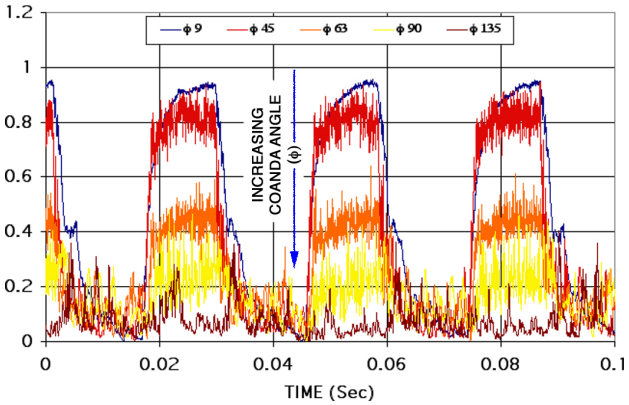

Figure 36 Time trace of pulsed jet along the Coanda surface (Driver frequency 35 Hz, 50% duty cycle, and h 0.020")

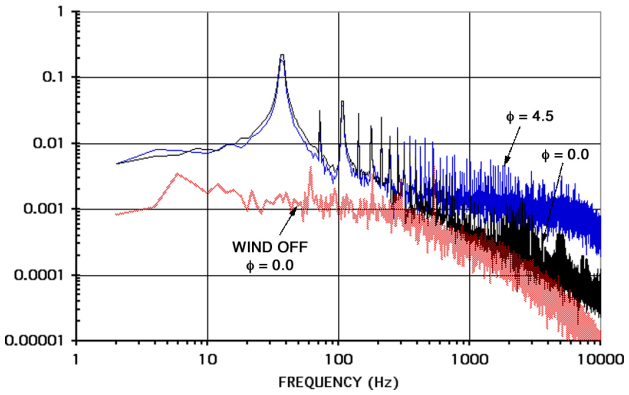

Figure 37 Spectra of the pulsed jet in the vicinity of the slot exit, (35 Hz, 50% duty cycle, and h 0.020")

Comparing the pulsed and steady lift performance of the GACC airfoil, figure 38, a distinct improvement in can be seen. For a given lift coefficient of 1.0, a 48% reduction in mass flow is realized for a 20% duty cycle. As the duty cycle is increased the performance benefit decreases. Comparing the lift performance of the pulsed and steady CCW at a fixed mass flow of 25 SCFM results in a 35% lift improvement.

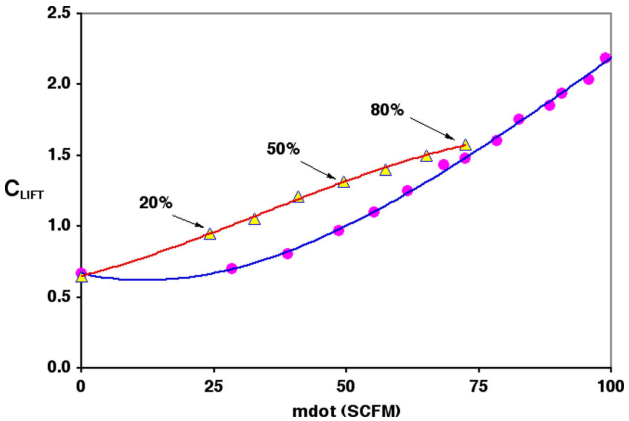

Figure 38 Comparison of pulsed and steady circulation control, (Frequency 35 Hz and varying Duty Cycle).

Concluding Remarks

The steady and pulsed aerodynamic performance of the GACC airfoil has been demonstrated using both CFD and experimental methods. The FUN2D code used in this study predicted the performance trends of the experiment very well and proved to be an excellent tool for identifying flow features that were subsequently probed in the experiment. The CFD results were also a valuable asset in interpreting the performance characteristics related to the Coanda jet and the GACC high lift configuration.

The baseline performance for the GACC high lift configuration is similar to other circulation control wings described in the literature. The performance of the pneumatic aileron in cruise conditions (i.e. dual blowing) showed significant improvements in drag over the unblown baseline configuration. Application of the GACC airfoil to a specific general aviation or personal vehicle may or may not be practical due to the large baseline drag. It is believed that the airfoil can be optimized to reduce the baseline drag but is not within the scope of this flow physics study.

This study has provided extensive details in the region of the Coanda surface and has identified issues related to the modeling of the Coanda jet. The isentropic expansion of the conditions at the jet exit quantifies jet velocities that are typically lower than the integrated velocity at the jet exit. The magnitude of this error is a function of the slot height and the internal development of the jet exit profile.

The difficulties in experimentally measuring the jet exit profile for the GACC airfoil is realized in the spatial resolution of the trailing edge. The physics of the jet velocity at the trailing edge, particularly at the jet exit are critically important in understanding the performance benefits of steady and pulsed pneumatic control of the GACC airfoil. The measured Coanda surface pressure profile identified a pressure peak at the slot exit that was consistent with CFD results. Using this pressure to quantify the jet velocity and momentum coefficient did not realize a collapse of the airfoil performance data. Further study is necessary, particularly for the compressible jets created when using small slot heights.

The performance of the pulsed blowing system realized a 50% reduction in required mass flow for a given lift coefficient. Variations in the duty cycle at a given frequency highlighted the controllability of the performance with small bursts of high-speed air. The study of the pulsed air delivery system identified losses related to the plenum volume and the performance requirement of the actuator itself. Continued research is necessary to quantify the overall system time dependent response of the GACC airfoil including the leading edge and internal plenums. Modifications to the internal flow path to improve the pulsed system authority will be necessary to increase the overall lift performance.

The GACC airfoil has been proven to be an excellent test bed for the multi-functional circulation control study that can operate as a high lift system, a pneumatic aileron, and a high-speed air brake. Follow-on testing is expected to improve the database for CFD validation and the understanding of the flow physics related to circulation control concepts.

INPUT PRESSURE: 100 PSIA					
FREQ	DUTY CYCLE				
	20%	25%	50%	75%	80%
25 HZ	0.8	1.0	2.1	3.1	3.3
50 HZ	0.7	1.0	2.0	3.1	3.3
100 HZ	0.7	0.9	2.0	3.0	3.2
150 HZ	0.5	0.7	1.8	3.0	3.3
200 HZ	0.0	0.2	2.0	3.1	3.7
	STANDARD CUBIC FEET PER MINUTE				

Table 1. Single actuator performance at inlet pressure of 100 psig

INPUT PRESSURE: 200 PSIA					
FREQ	DUTY CYCLE				
	20%	25%	50%	75%	80%
25 HZ	1.5	2.0	4.2	6.4	6.8
50 HZ	1.3	1.7	3.9	6.1	6.6
100 HZ	0.7	1.3	3.5	5.7	6.1
150 HZ	0.0	0.1	2.7	5.0	5.5
200 HZ	0.0	0.0	2.7	5.1	6.1
	STANDARD CUBIC FEET PER MINUTE				

Table 2. Single actuator performance at an inlet pressure of 200 psig

INPUT PRESSURE: 300 PSIA					
FREQ	DUTY CYCLE				
	20%	25%	50%	75%	80%
25 HZ	2.1	2.7	6.2	N/A	N/A
50 HZ	1.4	2.0	5.5	9.1	N/A
100 HZ	0.0	0.8	4.5	7.9	8.4
150 HZ	0.0	0.0	2.7	5.1	5.8
200 HZ	0.0	0.0	0.8	5.0	6.1
	STANDARD CUBIC FEET PER MINUTE				

Table 3. Single actuator performance at an inlet pressure of 300 psig

Component	Load
Normal	100 lb
Axial	5 lb
Pitch	400 in-lb
Roll	1200 in-lb
Yaw	40 in-lb

Table 4. Load limits of the GACC 5-component strain gage balance

Appendix

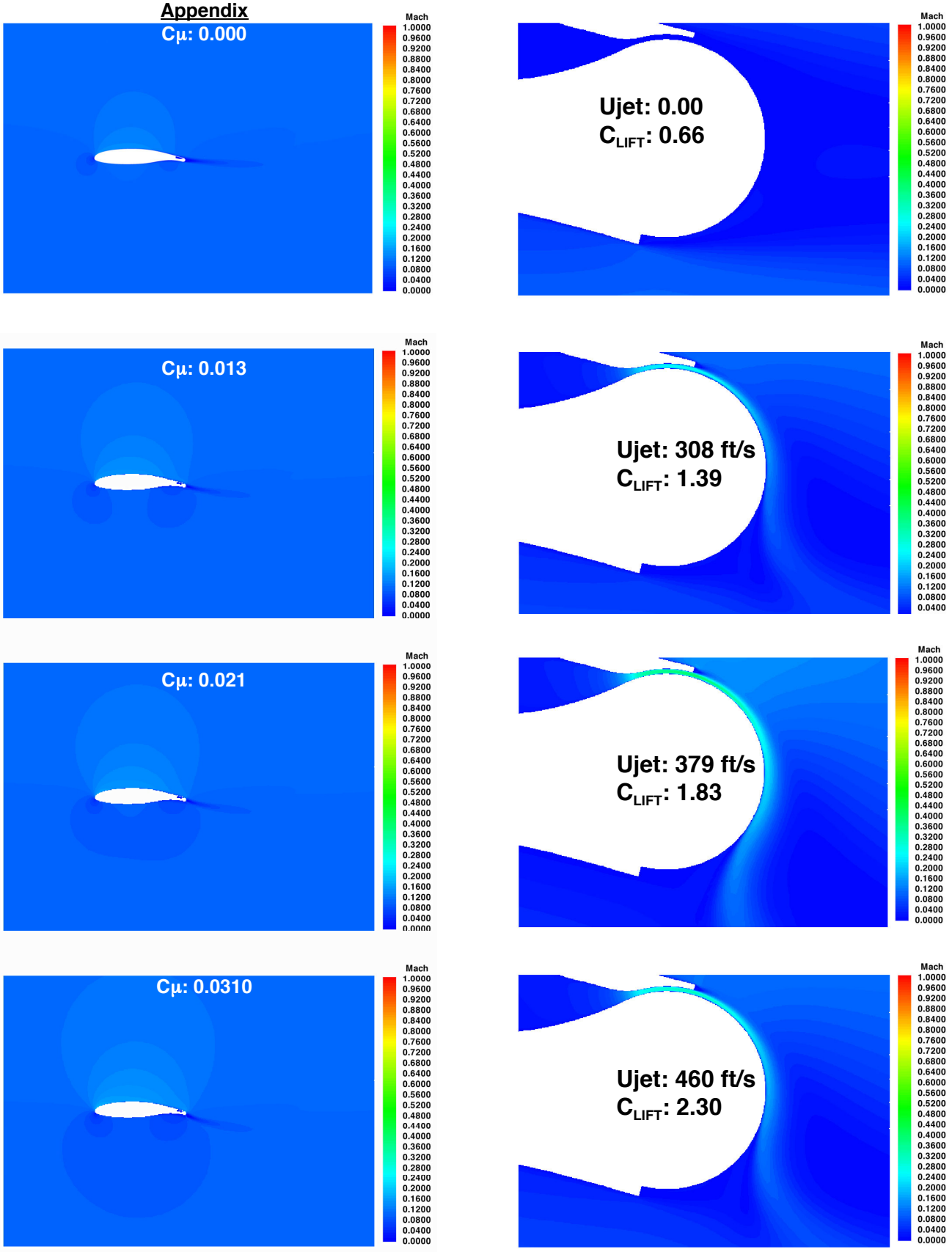

Appendix 1 Influence of Coanda Jet on the Mach number distribution

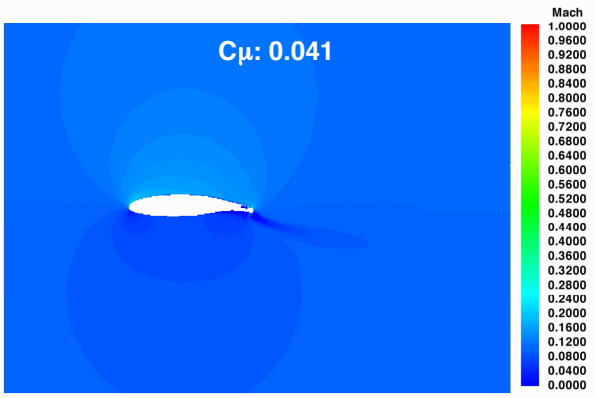

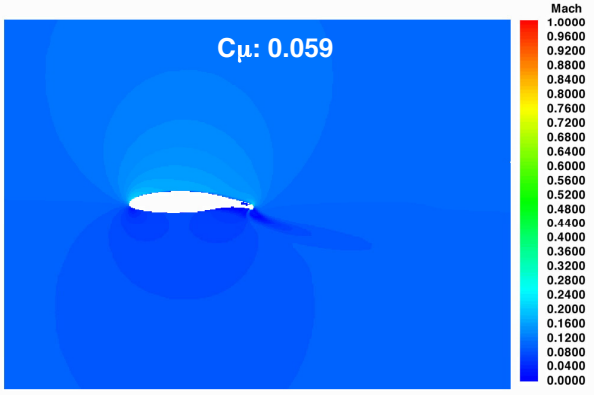

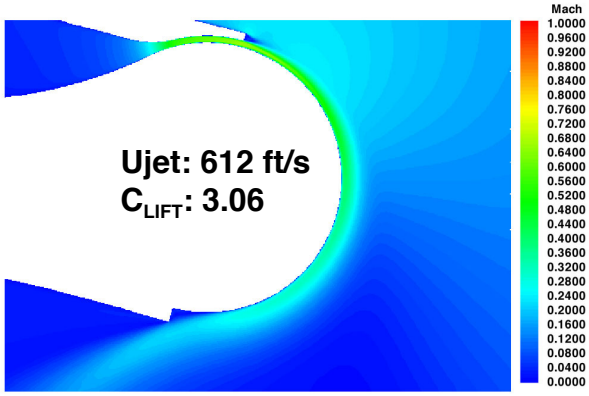

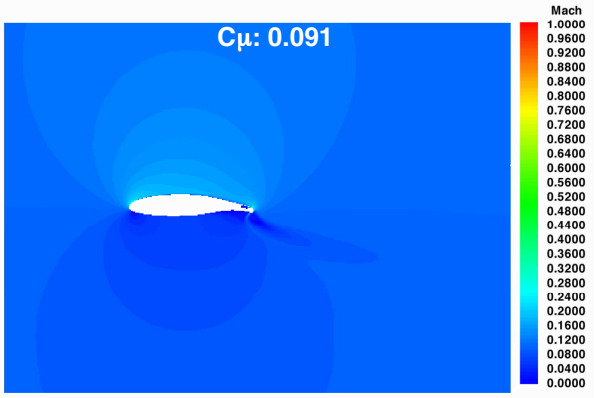

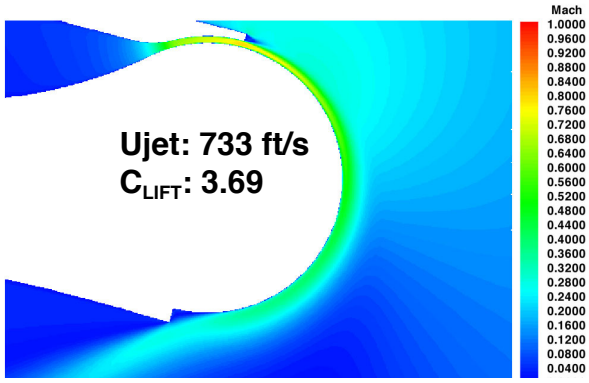

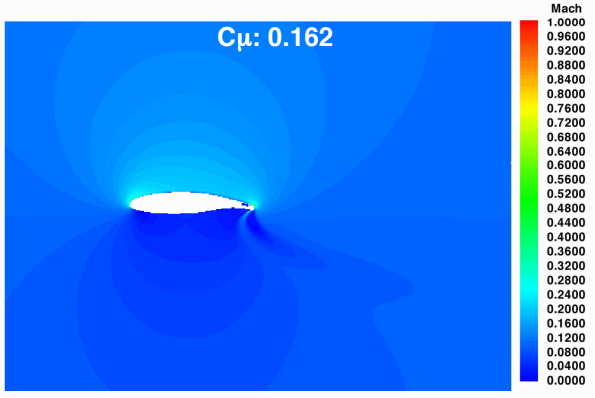

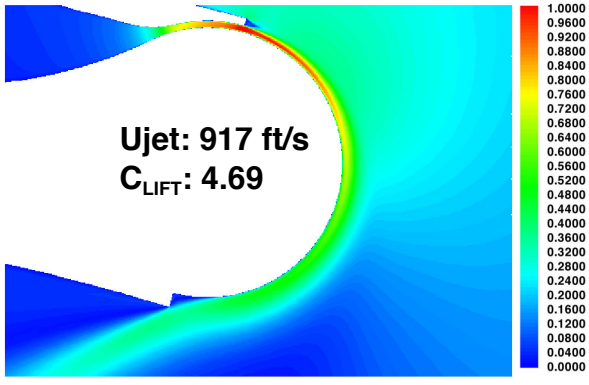

Appendix 1 Continued

References:

[1] Jones, G.S., Bangert, L.S., Garber, D.P., Huebner, L.D., McKinley, R.E., Stutton, K., Swanson, R.C., Weinstein, L., "Research Opportunities in Advanced Aerospace Concepts", NASA/ TM-2000-210547, December 2000

[2] Metral, A.R., "On the Phenomenon of Fluid Veins and their Application, the Coanda Effect," AF Translation, F-TS-786-RE, 1939

[3] Schlichting, H., "Boundary Layer Theory", page 750 – 751, 2nd Edition, 1979

[4] Karamcheti,K., "Principles of Ideal-Fluid Aerodynamics", John Wiley and Sons, Inc., page 376 – 401, 1966

[5] Wood, N., and J. Nielson, "Circulation Control Airfoils Past, Present, and Future," AIAA Paper 850204, January,1985.

[6] Englar, R.J., Circulation control Pneumatic Aerodynamics: blown force and Moment Augmentation and Modifications; Past, Present, & Future", AIAA 2000-2541, June 2000

[7] Liu, Y., Sankar, L.N., Englar, R.J., Ahuja, K.K., "Numerical Simulations of the Steady and Unsteady Aerodynamic Characteristics of a Circulation control Wing Airfoil," AIAA 2001-0704, January 2001

[8] Smith, A.M.O., "High Lift Aerodynamics, 37th Wright Brothers Lecture, AIAA 74-939, August 1974

[9] Anderson W.K., Bonhaus D.L., McGhee R.J., Walker B.S., "Navier–Stokes computations and experimental comparisons for multi-element airfoil configurations." J Aircraft 1995;32(6):1246–53.

[10] Englar, R.J., Circulation control – A Bibliography of DTNSRDC Research and selected Outside References., DTNSRDC-84/052, Sept 1984.

[11] Englar, R. J., "Development of the A-6 Circulation Control Wing Flight Demonstrator Configuration," DTNSRDC Report ASED-79/01, January, 1979.

[12] Oyler, T.E., Palmer, W.E., "Exploratory Investigation of Pulse Blowing for Boundary Layer Control", North American Rockwell Report NR72H-12, January 15, 1972

[13] Walters, R.E., Myer, D.P., & Holt, D.J., "Circulation Control by Steady and Pulsed Blowing for a Cambered Elliptical Airfoil", West Virginia University, Aerospace Engineering TR-32, July 1972

[14] Cagle, C.M., Jones, G.S. "A Wind Tunnel Model to Explore Unsteady Circulation Control for General Aviation Applications, AIAA 2002-3240, June 2002

[15] Rose, R.E., Hammer, J.M., & Kizilos, A.P., "Feasibility Study of a Bi-directional Jet Flap Device for Application to Helicopter Rotor Blades," Honeywell Document No. 12081-FR1, July 1971

[16] Englar, R.J., Williams, R.M., "Design of a Circulation Control Stern Plane for Submarine Applications," NSRDC Technical Note AL-200, March 1971

[17] Englar, R.J., Williams, R.M., "Test Techniques for High Lift, Two-Dimensional Airfoils with Boundary Layer and Circulation Control for Applications to Rotary Wing Aircraft", Canadian Aeronautics and Space Journal, Vol.19, No.3, March 1973

[18] Anderson, W. K., and Bonhaus, D. L., "An Implicit Upwind Algorithm for Computing Turbulent Flows on Unstructured Grids," Computers Fluids, Vol. 23, No. 1, 1994, pp. 1-21.

[19] Spalart, P. R., and Allmaras, S. R., "A One-Equation Turbulence Model for Aerodynamic Flows," AIAA Paper 92-0439, January 1992.

[20] Marcum, D. L., "Generation of Unstructured Grids for Viscous Flow Applications," AIAA Paper 95-0212, January 1995.

[21] Marcum, D. L., and Weatherhill, N. P., "Unstructured Grid Generation Using Iterative Point Insertion and Local Reconnection," AIAA Journal, Vol. 33, No. 9, September 1995.

[22] Wentz, W.H., Seetharam, H.C., "Development of a Fowler Flap System for a High Performance General Aviation Airfoil," NASA CR 2443, 1974

[23] Braden,J.A., Whipkey, R.R., Jones, G.S., Lilley, D.E., "Experimental Study of the Separating Confluent Boundary Layer," NASA CR 3655, June 1983

[24] Englar, R.J., "Low-Speed Aerodynamic Characteristics of a Small Fixed Trailing Edge Circulation Control Wing Configuration Fitted to a Supercritical Airfoil," DTNSRDC Report ASED-81/08, March 1981.

[25] van Dam, C.P., "The Aerodynamic design of Multi-Element High-Lift Systems for Transport Airplanes," Progress in Aerospace Sciences 28 (2002) 101-144

[26] Schaeffler, N.W., Hepner, T.E., Jones, G.S., Kegerise, M.A., "Overview of Active Flow Control Actuator Development at NASA Langley Research Center," AIAA 2002-3159, June 2002